Electroluminescence Test to Identify Defect Frequency in Photovoltaic Modules

Dayane Cynthia Pinto Oliveira[1], Amanda Gomes Barboza[1], Camila Fernanda Cardoso Teixeira[1], Nicholas Medeiros Lopes[1], João Fonseca de Mendonça[1], Alan Rodrigues de Sousa[1] and Samira de Azevedo Santos Emiliavaca[1]

[1]SENAI Innovation Institute for Renewable Energy, Natal (Brazil)

Abstract

Based on the technologies and solutions presented in the literature for identifying defects in photovoltaic modules, this study aims to correlate the identification of non-visual defect types in photovoltaic modules with the factors that caused them, using electroluminescence (EL) testing as an identification tool. Motivated by the potential for degradation and reduced performance of photovoltaic (PV) power plants caused by quality issues with photovoltaic modules, this study conducts a preliminary classification of defect categories present in a sample of modules that will be installed in a PV power plant. The experimental sample consisted of a batch of 84 monocrystalline silicon photovoltaic modules, divided into two groups: 48 bifacial modules with a rated power of 550 W and 36 monofacial modules with a rated power of 555 W. Through systematic defect classification, individual module profiling and analysis of the grey scale uniformity of modules with lower power performance, correlations between specific defect types and performance degradation were established. As a result, the sample predominantly presented defects related to cell quality and construction processes.

Keywords: Electroluminescence (EL), defect, photovoltaic modules, photovoltaic solar plant.

1. Introduction

Early detection of defects in photovoltaic modules using electroluminescence (EL) imaging has gained prominence in the literature as an effective evaluation method. Recent studies have demonstrated the effectiveness of this technique in identifying a range of problems, from microcracks (Dhimish and Holmes, 2019) to complex issues such as potential-induced degradation (Puranik & Gupta, 2022), thus offering significant advantages in characterizing the performance potential and durability of photovoltaic cells and modules. Quantitative analysis via EL, as presented in Rajput et al. (2018), facilitates the extraction of critical electrical parameters, such as series resistance and saturation current, thus enabling an accurate diagnosis of the condition of individual cells.

The electroluminescence principle is essentially the same as that of a light-emitting diode. The photovoltaic module cell behaves like a diode, and when powered by electric current, there is a radioactive recombination of carriers that causes light emission. Although the production of radiative emission is relatively low, it can be detected using specific sensors (Fuyuki et al., 2005). Electroluminescence allows the characterization of the uniformity of the cell areas and the photovoltaic module, enabling the identification of defects that are not visible to the naked eye.

The technical specification IEC TS 60904-13 (IEC, 2018) defines the guidelines for performing the EL test, such as the electrical polarization condition of the module, temperature, and image processing. According to the specification, the test consists of applying a direct polarization to the photovoltaic module from a direct current source, forcing the current to flow through the cells in order to generate light emission in the spectral range corresponding to the characteristic emission wavelength of the semiconductor material used to manufacture the photovoltaic (PV) cell. The camera used must have a filter that allows the spectral emission range of the semiconductor material to be captured and must be positioned perpendicular to the surface of the module to avoid interference from reflections and optical noise. The test must be carried out in a darkened, temperature-controlled environment. In addition, the use of lenses with filters that limit the capture of visible light is recommended.

Each module technology has a specific electroluminescent emission spectrum that must be aligned with the quantum efficiency of the sensor used in EL imaging. Crystalline silicon (c-Si) modules have spectral emission in the near-infrared range between 900 nm and 1300 nm, with an emission peak centered at approximately 1150 nm. Thin film technologies such as Cadmium Telluride (CdTe) have a peak around 830 nm, and materials such as amorphous

10.18086/swc.2025.03.25 Available at http://proceedings.ises.org

silicon (a-Si) and Copper Indium Gallium Selenide (CIGS) exhibit broader emission ranges. This difference indicates that the choice of sensor must be compatible with the spectral range of the material being analyzed to ensure adequate capture of the radiation emitted during the EL test.

In terms of quantum efficiency, Charge Coupled Device (CCD) and Complementary Metal Oxide Semiconductor (CMOS) sensors have a reduced response for crystalline silicon and CIGS modules, while the Indium Gallium Arsenide (InGaAs) sensor has high quantum efficiency between 900 nm and 1600 nm, fully covering the c-Si emission spectrum and providing greater sensitivity and lower noise in images. Despite this, even with limited spectral efficiency for accurate detection in the infrared range, sCMOS sensors are widely used due to their low cost and high resolution (Jahn et al., 2018). To optimize the capture of EL images from c-Si modules, mirrorless cameras with CMOS sensors are commercially adapted by removing the infrared filter (UV-IR), located near the camera sensor and responsible for limiting the capture of this range of the spectrum (Fada et al., 2016).

According to the review of failures of photovoltaic modules (Köntges et al., 2014), most defects observed through EL testing are the result of the manufacturing process, mechanical stress, environmental degradation, electrical interconnection failures, and cell integrity. The main defects detected are cracks in the cells, classified according to the degree of insulation compromise in the affected regions; defects in metal contacts such as defective or inactive fingers; interconnection failures such as shunt faults that compromise the electrical continuity of the module; potential-induced degradation (PID); moisture corrosion; and mechanical cracks caused by impacts.

Defects such as microcracks mainly originate during the manufacturing, transportation, and installation stages. During production, microcracks are usually microscopic and have a negligible initial impact on power, but they make the module more susceptible to future degradation. Depending on their severity, they are classified according to the level of electrical disconnection they cause. The impact of microcracks on performance and durability depends on their orientation and position in relation to the busbars, since parallel or branched cracks tend to cause electrical insulation and hot spots, while diagonal and perpendicular cracks have less impact on performance, unless they occur in a large number of cells (Picco et al., 2024). The identification and classification of these defects are essential for assessing the reliability, safety, and long-term performance of photovoltaic modules.

EL defect categorization keeps pace with advances in PV module technologies. A significant amount of work addresses the detailing and identification of defects in older technology modules, mainly because it focuses on degradation studies in modules that were already in operation (Berardone et al., 2018; da Fonseca et al., 2020). Recent studies approach defect identification, including the manufacturing stage. Some microcracks are generated at the cut edges of cut silicon cells (half or 1/3 cell), this defect occurs mainly during the laser ablation process, and although they do not have a significant initial impact on module performance, they can evolve into dendritic microcracks due to mechanical and thermal stresses during transport and installation (Köntges et al., 2025).

Advances in EL defect detection range from cost-effective image capture methodologies (Figueiredo et al., 2018) to automated systems based on artificial intelligence (Otamendi et al., 2021), which achieve over 99% accuracy in identifying anomalies. Berardone et al. (2018) demonstrate the effectiveness of the technique in real operating conditions, highlighting its ability to correlate EL patterns with various degradation mechanisms. Regarding the acceptance criteria for identified defects, the Brazilian standard ABNT NBR 17258 (ABNT, 2025), although not mandatory, establishes the criteria for electroluminescence inspection in c-Si photovoltaic modules, in accordance with the national market's need to ensure the quality of imported modules.

Problems documented in the literature, such as power loss in photovoltaic plants due to the appearance of microcracks (Bdour et al., 2020; Bakir, 2024) and the low quality of modules supplied to Brazil, highlight the need for inspections that go beyond power measurement tests. When evaluated in terms of large power plants, the trend of power loss gains greater prominence in view of the investment and generation expectations. Many companies seek electroluminescence analysis services after recording lower-than-expected generation results in a short period of time.

Thus, the importance of conducting pre-installation EL tests is emphasized, both to ensure the conformity of modules available on the market and to monitor possible defects during the operation of photovoltaic plants. The objective of this work is to analyze a batch of modules received from the electroluminescence test, observing the number of defects presented, establishing a correlation between the frequency of occurrence of defects with the factors that cause them (manufacturing, incorrect handling, or transportation) and their impact on performance.

2. Materials and Methods

2.1. Module Description and Sampling

For this study, a sample of 84 modules was considered: 48 bifacial modules with 550W of power and 36 monofacial modules with 555W of power. The two categories of modules, from the same manufacturer and belonging to the same technological family (c-Si), have an identical configuration of 144 mono PERC photovoltaic cells in half-cut architecture, with equivalent cell area and module dimensions. Both share similar construction, electrical, and mechanical characteristics, including comparable efficiency, current, and voltage parameters, as well as compliance with the same regulatory and qualification standards. The technical distinction between them lies in the irradiance capture nature, one being monofacial, restricted to the front face, and the other bifacial, also capable of converting radiation reflected by the rear surface.

The modules were obtained as part of a photovoltaic solar power plant project. From the total number of modules received, six modules were removed from each pallet to compose the sample analyzed. The selected modules underwent a cycle of standardized performance tests to ensure that a qualitative analysis by electroluminescence would not be influenced by any previously identified non-conformities. Visual inspection tests, insulation tests, and maximum power determination tests were performed in a solar simulator in accordance with IEC 61215.

2.2. Experimental Procedure

After the performance testing cycle, the electroluminescence (EL) test was performed on each of the photovoltaic modules using a camera with a CMOS sensor and IR filter removed, in accordance with IEC TS 60904-13. The procedure was divided into three stages: image acquisition (stage 1), defect identification (stage 2), and data processing (stage 3). Stage 1 consisted essentially of performing the test and capturing images with the EL camera. The modules were properly positioned on the mounting structure and polarized directly from a DC source, supplying them with a voltage equal to Voc (open circuit voltage) + 3 V and a current close to Isc (short circuit current). The image acquisition sequence consisted of one image of the entire module and close-up images of details relevant to the study.

Step 2 occurred simultaneously with step 1, consisting of marking each defect recorded, according to the established numerical scheme, in a table representing the module. Figure 1 illustrates the scheme adopted for identifying defects. The sequence of defects established for the sample was constructed in order of identification of each one. Ten categories of defects were classified from 1 to 10: Low Severity Microcrack; Dark Spot; High Severity Microcrack; Scratch on Glass; Defective Gridfingers; Scratch; Cluster of Dark Spots; Broken Gridfingers; Stain and Stain on Semiconductor.

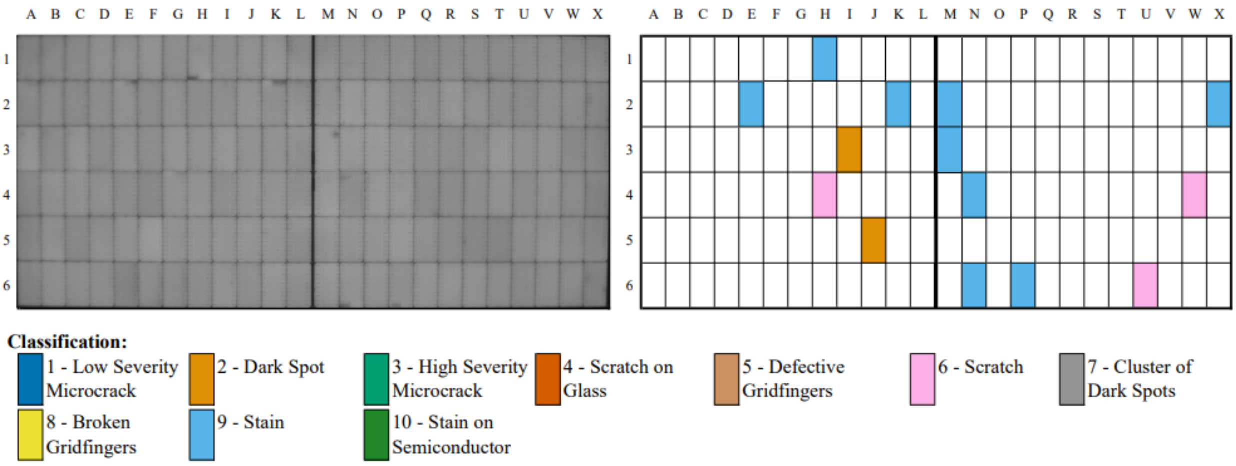

Figure 1: Identification model for electroluminescence defects in photovoltaic modules.

Table 1 details the defined defect categories. Defects in the Low Severity Microcrack category (Defect 1) include cells that have microcracks caused by crushing (due to pressure or mechanical impact), explosive cracks (which propagate in four directions), and diagonal cracks (which propagate along the cell). The types of defects grouped in this category impact cell performance, with mechanical and electrical risks associated with the propagation of these failures. The High Severity Microcrack (Defect 3) classification is intended to quantify microcracks with a greater potential to cause structural and efficiency damage than the Defect 1 category. It includes the occurrence of branched microcracks, which generally cover a larger area of the cell and have a network propagation pattern. This category may also include cells with other types of microcracks when they are extensive or when there is an association of more than one type of microcrack.

Table 1: Type of defect and corresponding defect image.

ID	Type	Image
1	Low Severity Microcrack	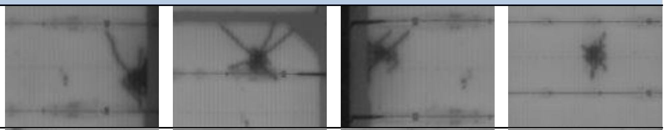
2	Dark Spot	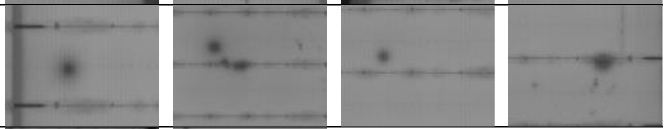
3	High Severity Microcrack	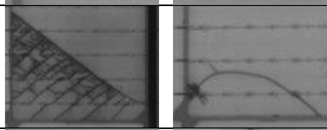
4	Scratch on Glass	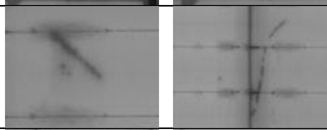
5	Defective Gridfingers	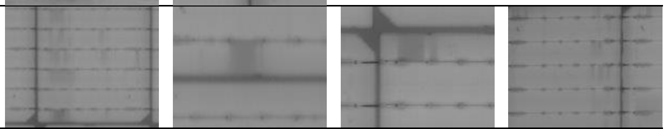
6	Scratch	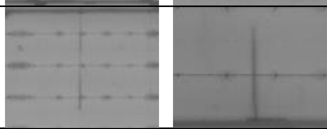
7	Cluster of Dark Spots	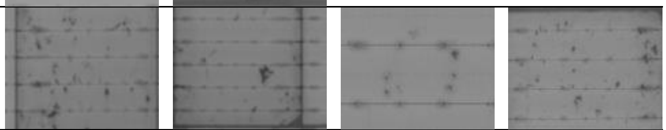
8	Broken Gridfingers	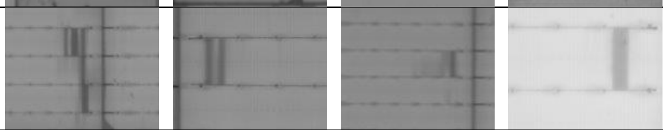
9	Stain	
10	Stain on Semiconductor	

The Dark Spot category includes small dark areas on the cell caused by impurities or defects in the cell, which when observed in greater quantity and proximity can be classified in the Cluster of Dark Spots category. Scratch on Glass classifies patterns of lines or marks on the glass also identifiable with EL, while Scratch refers to these occurrences on the cell surface. Defective Gridfingers can be classified as photovoltaic cell fingers with compromised performance, but which are not yet completely inactive, as in the case of Broken Gridfingers, which are characterized as missing or interrupted fingers, both cases directly influencing the overall efficiency of the cell. Cells with regions of low luminescence are classified as Stain and can be recorded at the edges, corners, or any position on the cell and are related to the manufacturing process. Stain on Semiconductor refers, by internal classification, to any defect visible to the naked eye in the semiconductor layer, as in the case recorded in Table 1, resulting from a small layer of solder deposited on the cell.

The third and final stage of the experimental procedure consisted of processing the data, using the tables completed in stage 2 to obtain information on the frequency of occurrence of defects and to draw up the defect profile for each module. The data from all tables were quantified, and the number of occurrences of each defect was estimated.

3. Results and Discussion

The frequency of defects observed in the EL test was analyzed from different perspectives, the first of which consisted of quantifying the defects. A total of 1,181 defects were recorded, and the graph in Figure 2 shows the total number of occurrences for each defect category. Category 9 had the highest number of records, accounting for 35.14% of the total. Next are categories 5 and 2, contributing 22.52% and 20.15% of the total occurrences, respectively. Approximately 78% of the occurrences belong to the categories Stain, Defect Gridfingers, and Dark Spot, indicating that most of the defects in the sample are related to the manufacturing process and quality of the cells used. The Cluster of Dark Spots (2.62%) and Broken Gridfingers (3.73%) categories are less representative, but are directly related to categories 5 and 2.

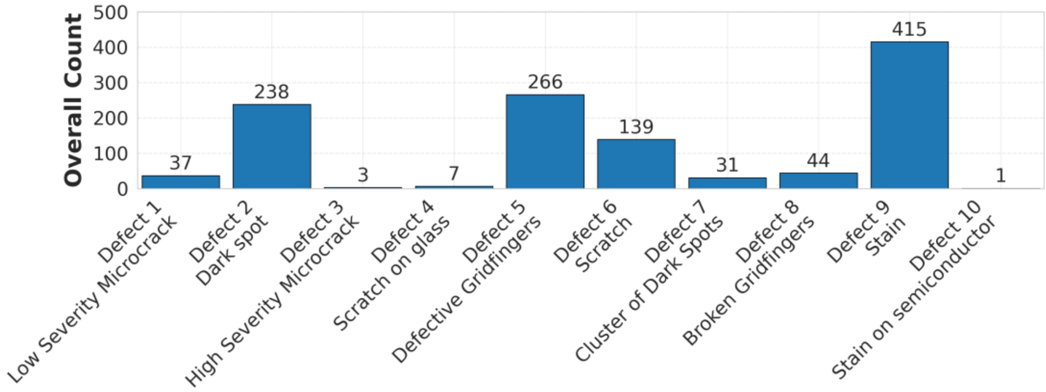

Figure 2: Total quantity by defect category.

The Scratch on Glass category does not occur frequently, accounting for 0.6% of cases. It includes physical defects in the module glass related to handling and transportation that are identifiable by EL images. Although it does not indicate potential damage to the cell, its registration was relevant to validate the classification of the Scratch category, a defect identified on the cell surface that corresponds to 11.7% of the total occurrence of defects. The category with the lowest occurrence, with only one registration, was Stain on Semiconductor, with a defect also visible to the naked eye and related to the manufacturing process.

The Low Severity Microcrack category has an occurrence of 3.13% and has high potential for expansion, with defects classified in this category potentially evolving into the High Severity Microcrack category, which, despite having an occurrence frequency of 0.25% in the sample, has the greatest potential to compromise cell performance, potentially electrically isolating some areas of the cell and even disqualifying a module from the sample according to the requirements of the ABNT NBR 17258:2025 standard.

As for individual analysis, the relationship that can be evaluated is that between the position and the type of defect, using each photovoltaic cell in the module as a position reference. For each defect category, it is possible to obtain the percentage of occurrence related to the position in the photovoltaic module. Defect 1, despite few occurrences, indicates a subtle trend for cells located immediately above and below the central interconnection region, where the bypass diodes and cables are located. Defects 2, 5, 6, 7, and 8 have a more random distribution and are usually caused by impact, material quality, soldering flaws, and the production process in general, and can be related to both the manufacturing and transportation stages.

Defects 3 and 10 did not show significant records to justify a position trend, and Defect 4 does not relate exactly to the cell, but rather to the module's glass layer. Defect 9, on the other hand, has the highest occurrence and the most defined trend among all categories. Greater frequencies of occurrence are recorded in the cells closest to the edges of the module and the central interconnection line, which is a result of the manufacturing process. In this context, the overall frequency of defects by position in the module can be related. The graph in Figure 3 shows the percentage of defects by module position, considering all categories. The overall trend in the position of cells with the highest occurrence of defects follows the trend of Defect 9, with a higher concentration in cells adjacent to the edges and the central interconnection region. It is worth noting that this is an initial characterization specific to the sample analyzed, seeking to trace patterns of defect occurrence and the proportion in which they are being identified.

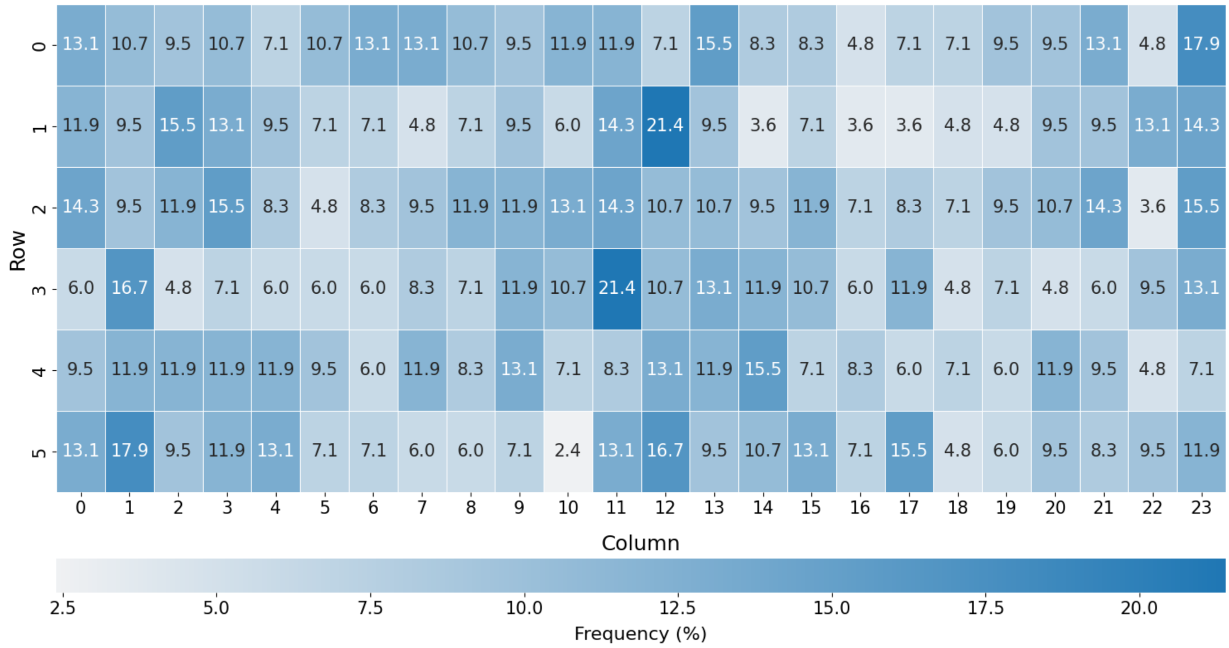

Figure 3: Frequency per module position (%) - All Defects (1 - 10).

The defect category distribution ratio in each module was also analyzed, considering that a module has 144 cells. The average number of defective cells per module was 9.8%, with a maximum value of 24.3% of defective cells in a single module. The distribution profile of these defects was qualitatively plotted for every module in the sample, with the 48 550 W modules shown in Figure 4 and the 36 555 W modules shown in Figure 5.

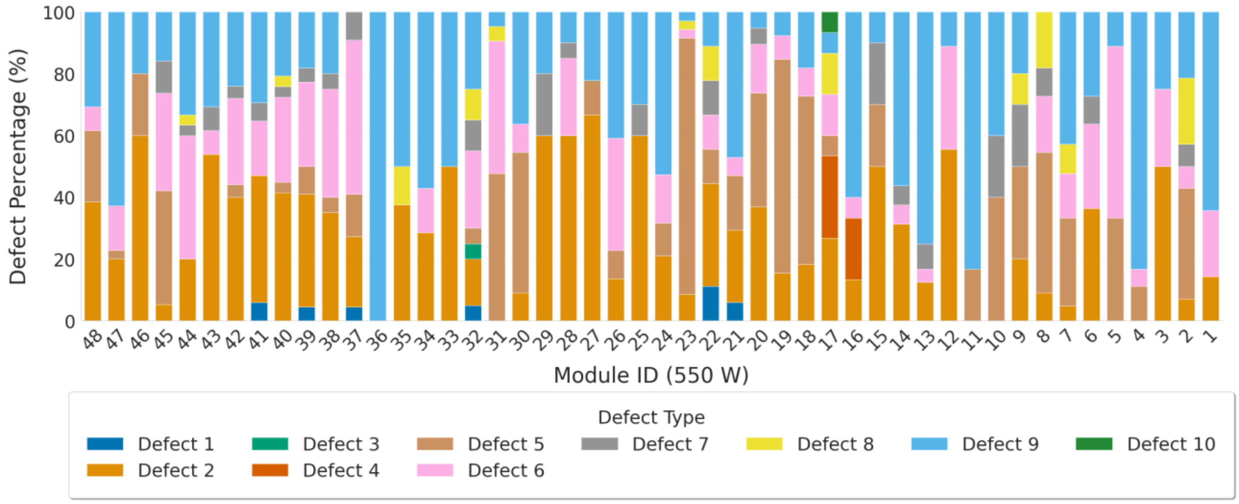

Figure 4: Defect distribution per PV module (550 W modules).

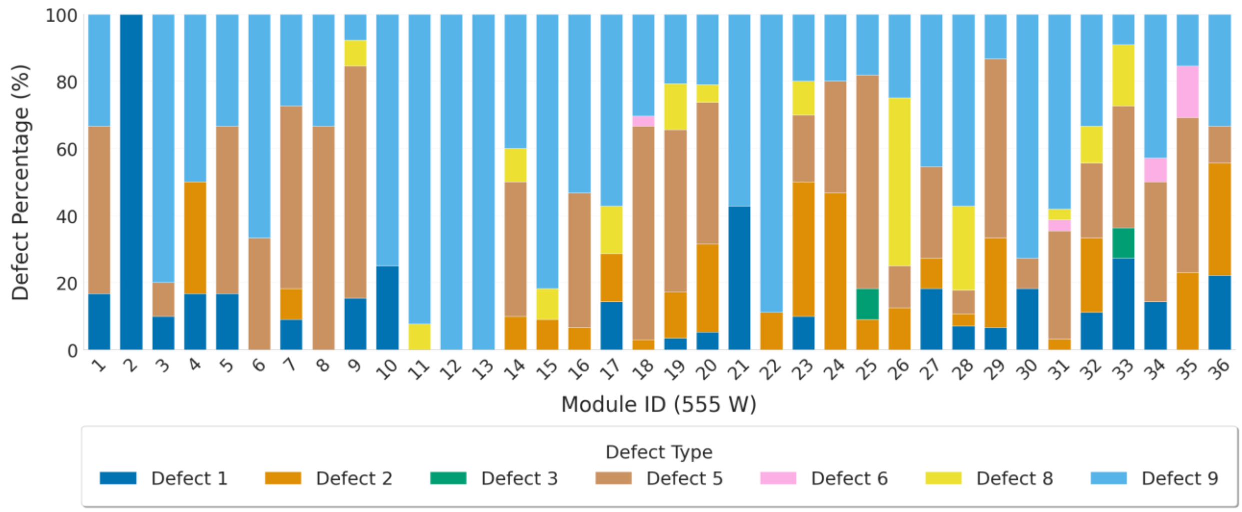

Figure 5: Defect distribution per PV module (555 W modules).

When aligned with module performance, information such as that shown in the graphs in Figures 4 and 5 can indicate how each defect category impacts performance. The power measurements of the modules are presented in Table 2. The values are in watts (W) and represent the average power between the direct and reverse power measurements of the modules. The maximum power determination test was conducted in accordance with IEC 61215-2 on a solar simulator classified as A+A+A+.

Table 2: Statistical summary of measured output power for 550 W and 555 W solar module samples.

Category	Number of Modules	Average Power (W)	Standard Deviation (W)	Minimum (W)	Maximum (W)
550 W	48	544.6	1.7	540.7	548.7
555 W	36	548.4	1.2	545.6	551.2

According to the data in Table 2, the standard deviation between the power values of the 550 W modules is slightly higher than the deviation of the power values of the 555 W modules. The sample's maximum and minimum power values were also recorded. For the sample of 550 W modules, the highest power value corresponds to module ID 12 and the lowest value to module ID 34. For the 555 W modules, module ID 29 recorded the highest power value, and module ID 25 recorded the lowest value. Although lower than the nominal power value, all measured power values are within the simulator's uncertainty range.

Module ID 34 (550W) has defects 2, 6, and 9, with defect 9 being the most prevalent. Module ID 25 has defects 2, 3, 5, and 9, with defect 5 being the most prevalent. To parameterize the influence of the types of defects listed, an analysis of the uniformity of luminance emission of the cells in the modules with the worst and best performance in the sample was also performed based on this information. The electroluminescence photos of the four selected modules were digitally processed to calculate the homogeneity between the coloring of the cells. The purpose of this analysis was to calculate the percentage of cells with low luminance in these modules. The ABNT NBR 17258:2025 standard establishes the acceptance criteria that allows up to 10% of cells with differences in the gray scale between 25% and 40%, with values above this range and color variations greater than 40% resulting in the module being rejected.

In the uniformity analysis, the images were loaded and converted from RGB to 8-bit grayscale, preserving the light intensity of each pixel. Next, Contrast Limited Adaptive Histogram Equalization (CLAHE) was applied to enhance local contrast, highlighting subtle variations in brightness between cells. Each image was segmented into individual cells (6x24), and the intensity of each cell was calculated, allowing the lightest and darkest cells to be identified. From these values, luminance differences were calculated according to eq. 1 (ABNT NBR 17258:2025):

$$\text{Grayscale difference}(\%) = \frac{(\text{Cell with highest RGB value} - \text{RGB of the cell to be evaluated})}{255} x\, 100 \quad \text{(eq. 1)}$$

Cells with gray scale differences greater than 25% were considered to have low luminance. Figure 6 shows the results of the analysis, with the photo of the module followed by the graph showing the percentage difference in gray scale for each cell. According to the criteria used, the percentage of cells with low luminance for module ID 34 (550 W) was 3.5%, with a maximum measured power of 540.7 W (Figure 6a). The ID 12 module (550 W) recorded a maximum measured power of 548.7 W, with 0% of cells with low luminance (Figure 6b). The percentage of cells with low luminance for the ID 25 module (555 W) was 0.7%, with a maximum measured power of 545.6 W (Figure 6c), while the ID 29 module (555 W) recorded a maximum power of 551.2 W, with 0% of cells with low luminance (Figure 6d).

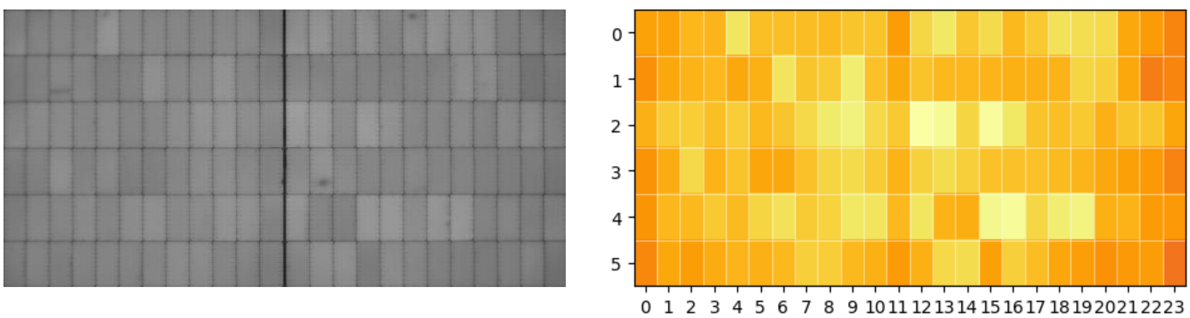

(a)

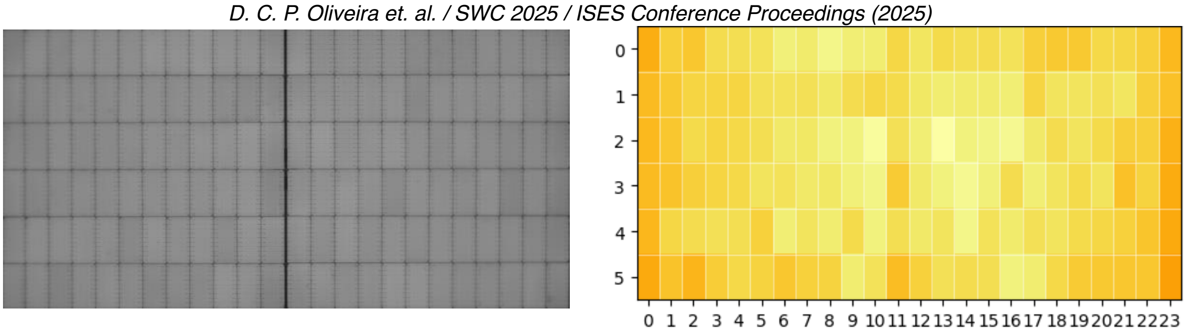

(b)

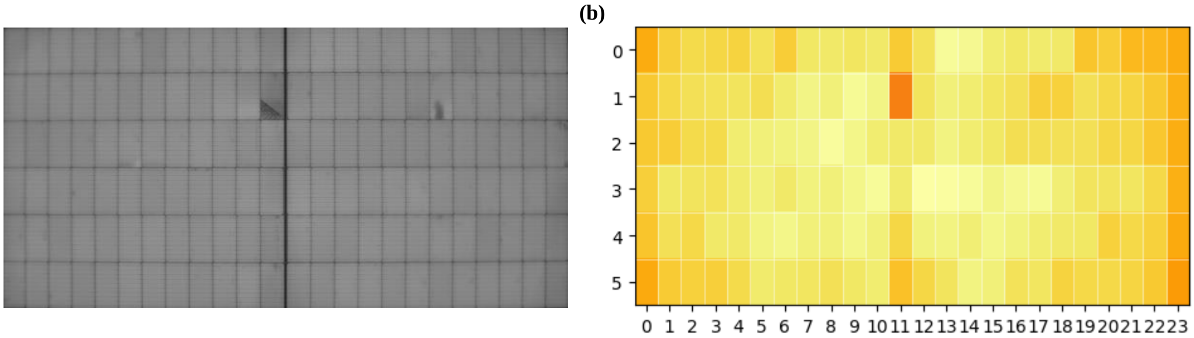

(c)

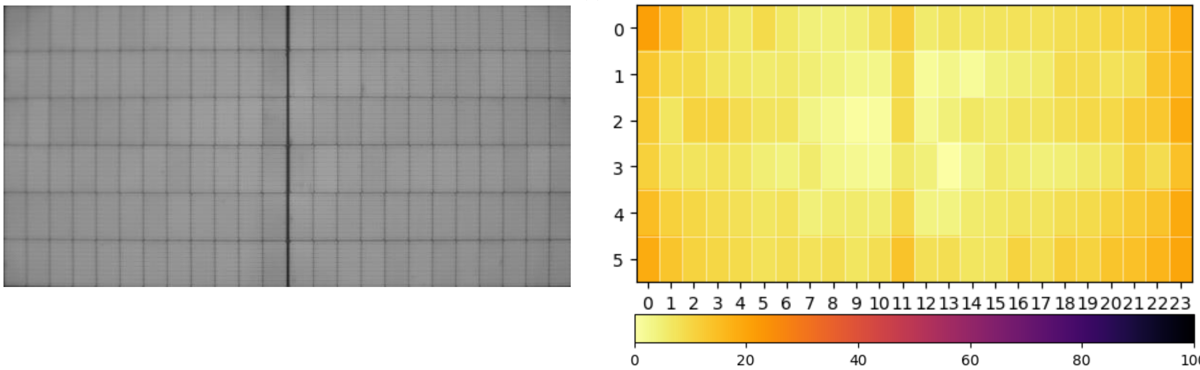

(d)

Figure 6: Module image and graph showing percentage difference in grayscale of each cell – (a) module ID 34 (550 W), (b) module ID 12 (550 W), (c) module ID 25 (555 W), and (d) module ID 29 (555 W).

Based on the requirements of the ABNT NBR 17258:2025 standard, all modules were compliant in terms of gray scale variation of the cells, with no cases of variation greater than 40% or modules with more than 10% of cells with differences between 25% and 40%. The worst-performing modules have few defects, but one has a higher percentage of non-uniformity in cell luminance levels, and the other has a High Severity Microcrack defect, with a branched microcrack (Figure 6c). Thus, a high severity defect and a higher luminance non-uniformity rate were equivalent in terms of module performance decline. Results such as these reinforce the importance of jointly analyzing the appearance and evolution of defects and cell efficiency based on the difference in grayscale. While module ID 25 (555 W) presents a defect that is not permitted according to the electroluminescence inspection criteria for photovoltaic modules, due to its greater potential impact on module efficiency, module ID 34 (550 W) still meets the criteria, despite having the worst performance in the 550 W category.

Although their power values fell within the simulator's uncertainty range, all modules in the sample had power values lower than those declared by the manufacturer, which can be attributed mainly, based on the electroluminescence results, to the quality of the cells and the manufacturing process. This finding is reinforced by a survey by TÜV Rheinland (2025), which compared performance data from photovoltaic modules tested between 2015/2016 and 2024, identifying that the proportion of PV modules delivering less power than stated doubled in ten years. Currently, about two-thirds of modules have lower than nominal power, while only one-third exceed the specified value. Although most results are in line with laboratory uncertainty, the study highlights the risk of loss of market confidence, recommending regular independent testing during the manufacturing stage.

4. Conclusion

The results show that electroluminescence inspection is an essential tool for assessing the quality and reliability of photovoltaic modules, allowing the identification of defects that would not be detected by conventional electrical tests alone. Analysis of the sample revealed the occurrence of various types of defects distributed unevenly among the cells, with emphasis on Stain (Defect 9), whose highest frequency was observed in regions close to the edges and the central interconnection line of the modules. This trend suggests a strong correlation with aspects of the manufacturing process, pointing to low cell quality and problems in the construction process. In addition to the defect categories with the greatest impact, recording defects on a smaller scale or with less impact was intended to characterize the sample and form a database for future identification in new modules.

The results reinforce that only measured power compliance with the stated uncertainty range does not guarantee the integrity and durability of photovoltaic modules. Even modules within acceptable limits showed signs of potential degradation, either due to severe microcracks or high non-uniformity in cell luminance. The correlation between high-severity defects and reduced performance indicates the need for continuous monitoring and EL testing both in the pre-installation phase and during operation. Thus, systematic inspection by electroluminescence, combined with electrical performance analysis, constitutes an integrated quality control approach, which is essential to ensure the reliability, efficiency, and longevity of photovoltaic systems.

Future work could include monitoring EL defects in the sample throughout the plant's operation, seeking to identify possible developments and impacts on performance. As required by the investigation, a more expanded defect classification methodology could be developed, dividing the categories into subcategories, or a more restrictive one, grouping qualitatively similar defects. In addition, a uniformity analysis of the gray scale of the modules can be conducted for the entire sample, as well as a detailed conformity classification of each defect category according to the criteria of ABNT NBR 17258:2025.

5. Acknowledgments

Research work carried out in the context of the activities of the National Institute for Technological Development of Photovoltaic Solar Energy Applications, INCT-DAESF, CNPq/MCTI/Brazil, Process 408486/2024-4. The authors would like to thank the SENAI Institute for Innovation in Renewable Energy for its support and infrastructure, CTG Brazil for its financial contribution to the ANEEL PD-10381-0620/2020 project, and TotalEnergies for its current financial contribution to the ANP 23980-6 and ANP 24118-2 projects.

6. References

Associação Brasileira de Normas Técnicas, 2025. ABNT NBR 17258:2025 — Critérios de inspeção de eletroluminescência em módulos fotovoltaicos. Rio de Janeiro.

Bakir, H., 2024. Detection of micro-cracks in PV system using electroluminescence (EL) testing. Niğde Ömer Halisdemir Üniversitesi Mühendislik Bilimleri Dergisi, 13(2), 1-1.

Bdour, M., Dalala, Z., Al-Addous, M., Radaideh, A., & Al-Sadi, A., 2020. A Comprehensive Evaluation on Types of Microcracks and Possible Effects on Power Degradation in Photovoltaic Solar Panels. Sustainability, 12(16), 6416. https://doi.org/10.3390/su12166416

Berardone, I., Garcia, J. L., & Paggi, M., 2018. Analysis of electroluminescence and infrared thermal images of monocrystalline silicon photovoltaic modules after 20 years of outdoor use in a solar vehicle. Solar Energy, 173, 478-486.

Berardone, I., Garcia, J.L., Paggi, M., 2018. Analysis of electroluminescence and infrared thermal images of monocrystalline silicon photovoltaic modules after 20 years of outdoor use in a solar vehicle. Solar Energy 173, 478-486.

da Fonseca, J. E. F., de Oliveira, F. S., Prieb, C. W. M., & Krenzinger, A., 2020. Degradation analysis of a photovoltaic generator after operating for 15 years in southern Brazil. Solar Energy, 196, 196-206.

Dhimish, M., Holmes, V., 2019. Solar cells micro crack detection technique using state-of-the-art electroluminescence imaging. Journal of Science: Advanced Materials and Devices 4, 499-508.

Fada, J. S., Wheeler, N. R., Zabiyaka, D., Goel, N., Peshek, T. J., and French, R. H., 2016. Democratizing an electroluminescence imaging apparatus and analytics project for widespread data acquisition in photovoltaic materials, Rev. Sci. Instrum., vol. 87, no. 8, p. 85109.

Figueiredo, G., Almeida, M.P., Manito, A., Zilles, R., 2018. Alternativa de baixo custo para imagens em eletroluminescência de módulos fotovoltaicos. In: Anais Congresso Brasileiro de Energia Solar-CBENS.

Fuyuki, T., Kondo, H., Yamazaki, T., Takahashi, Y., and Uraoka, Y., 2005. Photographic surveying of minority carrier diffusion length in polycrystalline silicon solar cells by electroluminescence, Applied Physics Letters, vol. 86, p. 262108.

IEC, T. S., 2018. 60904-13: 2018 Photovoltaic Devices—Part 13: Electroluminescence of Photovoltaic Modules. IEC: Geneva, Switzerland.

International Electrotechnical Commission, 2018. IEC TS 60904-13: Photovoltaic devices – Part 13: Electroluminescence of photovoltaic modules.

International Electrotechnical Commission, 2021. IEC 61215: Terrestrial Photovoltaic (PV) Modules: Design Qualification and Type Approval—Part. 2: Test. Procedures, Edition 2.0; International Electrotechnical Commission: Geneva, Switzerland.

Jahn, U., et al., 2018. Report IEA-PVPS T13-10: 2018-Review on Infrared and Electroluminescence Imaging for PV Field Applications. International Energy Agency.

Köntges, M., et al., 2014. Review of Failures of Photovoltaic Modules-Report IEA-PVPS T13-01: 2014. International Energy Agency-Photovoltaic Power Systems Programme.

Köntges, M., et al., 2025. Degradation and failure modes in new photovoltaic cell and module technologies. Report IEA-PVPS.

Otamendi, U., Martinez, I., Quartulli, M., Olaizola, I.G., Viles, E., Cambarau, W., 2021. Segmentation of cell-level anomalies in electroluminescence images of photovoltaic modules. Solar Energy 220, 914-926.

Picco, I. U., do Carmo, M. B., Rocha, G. P. U., Pereira, G. N., Sosa, C. D. F., do Rêgo Brandão, C. V., & Bonetto, M., 2024. Identificação e classificação de microtrincas em módulos fotovoltaicos através de teste de eletroluminescência. Revista Brasileira de Energia Solar, 15(2), 162-171.

Puranik, V.E., Gupta, R., 2022. Analysis and insight of electroluminescence imaging in the assessment of potential-induced degradation in crystalline silicon photovoltaic module. Engineering Failure Analysis 134, 106027.

Rajput, A.S., Ho, J.W., Zhang, Y., Nalluri, S., Aberle, A.G., 2018. Quantitative estimation of electrical performance parameters of individual solar cells in silicon photovoltaic modules using electroluminescence imaging. Solar Energy 173, 201-208.

TÜV Rheinland, 2025. Solar check – long-term trends: 10-year comparison of test data. Cologne, Germany: TÜV Rheinland, 5 May 2025. Available at: https://www.tuv.com/press/en/press-releases/solar-check-long-term-trends.html (Accessed: 02 October 2025).